Electron Microscopic Study of Soot Particulate Matter Emissions from Aircraft Turbine Engines

ARTICLE *in* ENVIRONMENTAL SCIENCE AND TECHNOLOGY · SEPTEMBER 2014

Impact Factor: 5.33 · DOI: 10.1021/es501809b · Source: PubMed

Environmental Science & Technology

Article

pubs.acs.org/est

Electron Microscopic Study of Soot Particulate Matter Emissions from Aircraft Turbine Engines

Anthi Liati,*[,†] Benjamin T. Brem,[‡,§] Lukas Durdina,[‡,§] Melanie Vögtli,[‡,§] Yadira Arroyo Rojas Dasilva,[∥] Panayotis Dimopoulos Eggenschwiler,[†] and Jing Wang[‡,§]

[†]Laboratory of Internal Combustion Engines, [‡]Laboratory of Analytical Chemistry, and [∥]Electron Microscopy Center, Empa Material Science and Technology, CH-8600 Dübendorf, Switzerland

[§]Institute of Environmental Engineering (IfU), ETH Zürich, CH-8093 Zürich, Switzerland

Supporting Information

ABSTRACT: The microscopic characteristics of soot particulate matter (PM) in gas turbine exhaust are critical for an accurate assessment of the potential impacts of the aviation industry on the environment and human health. The morphology and internal structure of soot particles emitted from a CFM 56-7B26/3 turbofan engine were analyzed in an electron microscopic study, down to the nanoscale, for ∼100%, ∼65%, and ∼7% static engine thrust as a proxy for takeoff, cruising, and taxiing, respectively. Sampling was performed directly on transmission electron microscopy (TEM) grids with a state-of-the-art sampling system designed for nonvolatile particulate matter. The electron microscopy results reveal that ∼100% thrust produces the highest amount of soot, the highest soot particle volume, and the largest and most crystalline primary soot particles with the lowest oxidative reactivity. The opposite is the case for soot produced during taxiing, where primary soot particles are smallest and most reactive and the soot amount and volume are lowest. The microscopic characteristics of cruising condition soot resemble the ones of the ∼100% thrust conditions, but they are more moderate. Real time online measurements of number and mass concentration show also a clear correlation with engine thrust level, comparable with the TEM study. The results of the present work, in particular the small size of primary soot particles present in the exhaust (modes of 24, 20, and 13 nm in diameter for ∼100%, ∼65% and ∼7% engine thrust, respectively) could be a concern for human health and the environment and merit further study. This work further emphasizes the significance of the detailed morphological characteristics of soot for assessing environmental impacts.

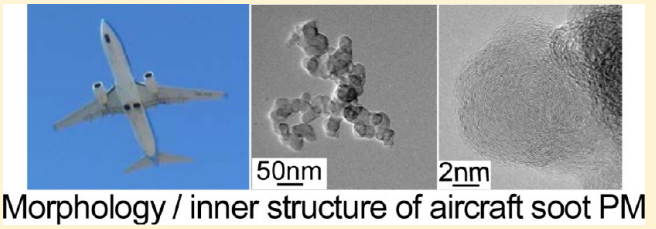

INTRODUCTION

Aircraft emissions contribute to local and global air pollution, potentially causing environmental and human health concerns. There is ample evidence that particulate matter (PM) emissions of aircraft operations can influence the Earth's radiative balance and climate via direct and indirect positive radiative forcing.[1] Potential impacts on human health are an increasing concern when airports are located close to urban areas and/or air traffic is growing as it has in recent years.[2] Reduction of soot PM emissions could potentially provide various health, climate, and food security benefits.[3−5] Properties of emitted soot particles that are relevant to their behavior in the atmosphere and the human body are associated with their morphology including size, shape, internal structure, and chemical composition.[6]

Data on aircraft soot emissions are generally scarce. To date, aircraft gas turbine engines whose rated maximum thrust is greater than 26.7 kN are regulated for gaseous emissions. All gas turbines, irrespective of thrust, are regulated for smoke. The so-called smoke number regulation was introduced in 1983[7] to reduce visible smoke trails from engines. Although the smoke regulation was intended as a visibility criteria, it also potentially reduced the nonvolatile PM mass emitted, but currently aviation PM emissions including nonvolatile ultrafine particles are not under regulatory control. Only recently, with a new potential emission standard in preparation,[8] a number of studies have performed measurements of PM mass and number emissions,[9−13] while few studies have addressed the detailed microscopic characterization of soot PM emitted.[14,15]

Within the framework of the present study, a series of experiments were carried out with a CFM 56-7B26/3 turbofan engine at the engine test cell of SR Technics, Zürich-Airport, where a permanent PM sampling system is installed. This work focuses on the electron microscopic study of the detailed morphological characteristics of soot particle emissions produced from the aircraft engine at three different levels of engine static thrust (takeoff, cruising, and taxiing) and on variations of these properties with the above thrust levels. In-depth knowledge of the morphology of soot emissions is expected to contribute to a better understanding of the particles' behavior in the atmosphere and the human body, as well as to mitigation strategies. For comparison with the

Received: April 11, 2014
Revised: July 18, 2014
Accepted: August 21, 2014

   dx.doi.org/10.1021/es501809b | Environ. Sci. Technol. XXXX, XXX, XXX−XXX

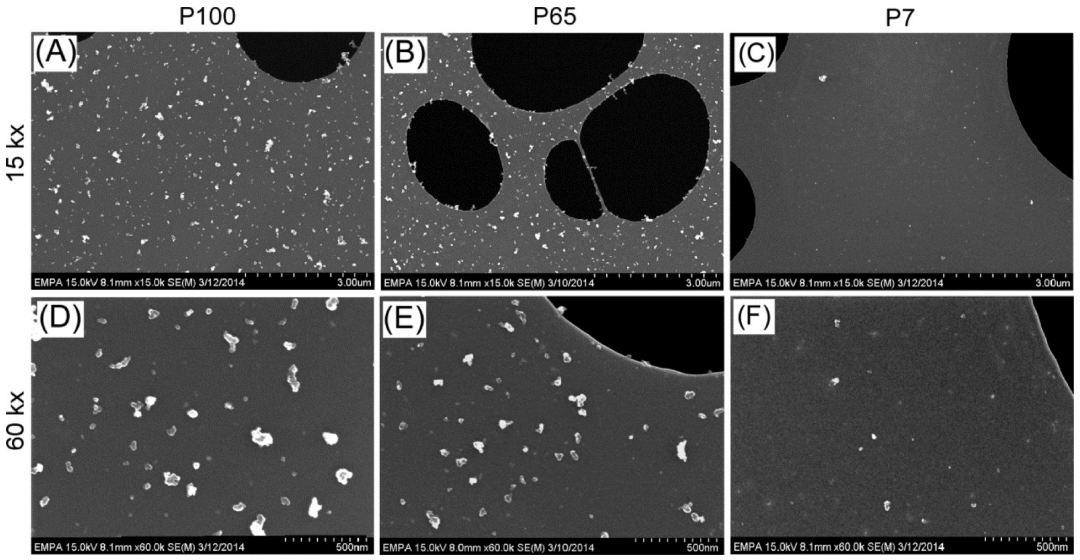

Figure 1. Secondary electron SEM images of samples collected at ~100% (A, D), ~65% (B, E), and ~7% (C, F) thrust level at 15 000 (A–C) and 60 000 (D–F) magnifications, showing a diminishing amount of soot agglomerates (bright particles on images) with reduced thrust level.

electron microscopic analyses, the concentration data and emission indices of nonvolatile PM mass and number are also reported for the selected engine conditions.

The soot morphological characteristics were studied by means of transmission electron microscopy (TEM) including the associated energy dispersive X-ray system (EDX) for qualitative chemical analyses and, to a minor part, by scanning electron microscopy (SEM). A significant advantage of the TEM characterization methods is that they apply high magnification and high resolution to physically examine the collected particles, determine important details of their morphology and internal structure, and directly measure the real sizes of the agglomerates and of their primary particle constituents down to the nanometer or even subnanometer scale. At this level of morphological detail, the sampling and especially the analytical time for TEM are quite substantial. As a consequence, the number of examined samples are not numerous and the statistics not optimal. In contrast, particle number and size analyzers, which are commonly used for measuring emissions, are rather suited for real-time online measurements, are less time-consuming, and provide better statistics, but they cannot go into the specific morphological details described above.[16,17]

■ EXPERIMENTAL SECTION

The experiments described in this paper were a part of the Aircraft Particulate Regulatory Instrumentation Demonstration Experiment (APRIDE 5) campaign that was conducted in July and August 2013 at SR Technics Zürich-Airport. While most of the campaign focused on the intercomparison of measurement systems that were built according to the currently under development aircraft exhaust sampling standard,[8] a targeted effort was made during a dedicated engine run to collect the TEM samples used for this work.

Setup and Sampling Procedures. *Engine and Test Matrix.* The emissions were measured from an in-service CFM 56-7B26/3 hi-bypass turbofan engine burning standard Jet A-1 fuel. This engine is popular in the current aircraft fleet and is used on the Boeing 737 short- to medium-range twinjet narrow-body airliner. The particular engine used had 2000 flight cycles (5009 h wing time) and had a stable performance during the entire campaign.

The test started with a 25 min warm-up sequence that included engine idle (3%), 7%, 15%, 65%, and 85% relative static engine thrust levels of 5 min each. After the warm-up sequence the TEM samples were collected at the three thrust levels listed in Supporting Information (SI) Table 1 running from high to low engine powers. The engine thrust levels were controlled according to the engine combustor inlet temperature (T3, proprietary value) for which the corresponding thrust levels are known for standard atmospheric conditions (15 °C, 1013.25 hPa). While the actual thrust is a function of ambient temperature and pressure, the method to control the engine by T3 is commonly used in the engine certification for gaseous emissions and visible smoke to report sea level corrected emissions data. Slight differences between the targeted and achieved control values (SI Table 1) are caused by limitations to set the T3 closer than ±1 °C to the target value and by drifts of up to 1.6 °C during long (30 min) run points.

Sampling. The sampling of aircraft gas turbine exhaust is challenging due to the high temperatures up to 850 °C and velocities up to Mach 1. A detailed description and an overview of the sampling system is provided in the Supporting Information and graphically illustrated in SI Figure 1. The TEM grids were collected in parallel to the other PM instrumentation with a nanometer aerosol sampler (NAS, 3089, TSI) setup outlined in SI Figure 1. Three TEM grids with loading times of 2, 3, and 6 min were collected for each of the three engine thrust points investigated in the present study, namely ~100%, ~65%, and ~7% static engine thrust as a proxy for takeoff, cruising, and taxiing, respectively. In order to get information on background soot emissions, two TEM grids were exposed for 2 and 5 min in the sampling line without running engine, but otherwise identical sampling conditions.

Electron Microscopic Methods of PM Study. TEM studies were performed with a JEOL 2200FS TEM/STEM microscope equipped with an Omega filter, a Schottky field emission gun at 200 kV, and a point to point resolution of 0.23 nm (Electron Microscopy Center of Empa). The TEM instrument is equipped with an EDX detector (JEOL EDX

dx.doi.org/10.1021/es501809b | Environ. Sci. Technol. XXXX, XXX, XXX–XXX

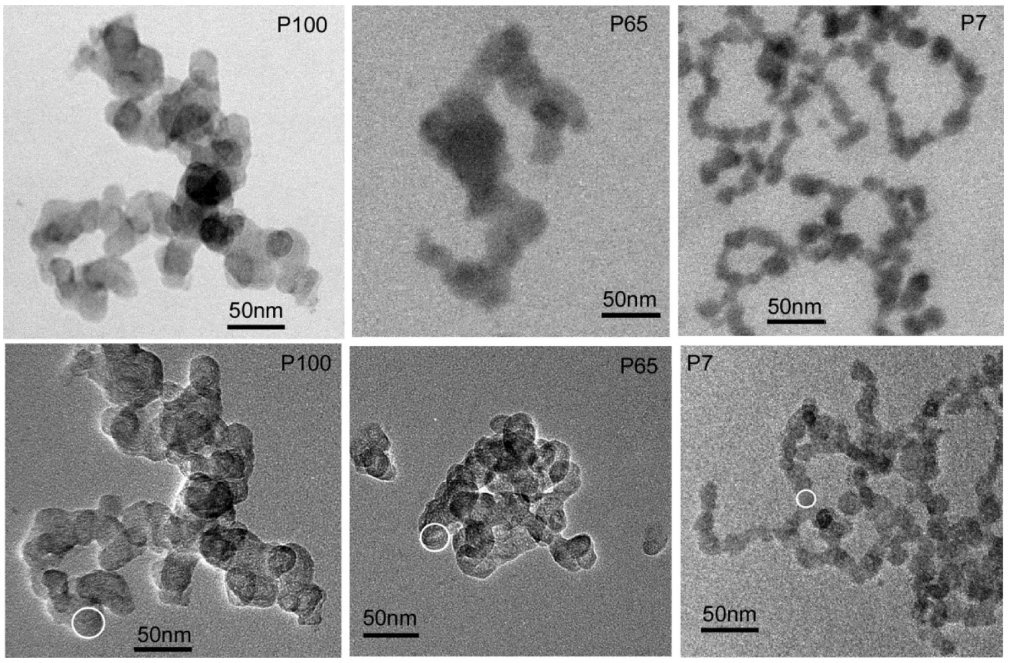

Figure 2. BF-STEM mode (upper row) and TEM mode images (lower row) of soot agglomerates from different engine thrust levels exhibiting a diminishing size of the primary soot particles from the higher to the lower thrust. Note the significantly smaller size of primary soot particles in the ~7% soot as compared to the ~65% and the ~100% thrust samples, as well as the less bulky agglomerates of the ~7% thrust soot. Encircled in the lower row images are examples of primary particles considered for size measurements.

detector: EX-24065JGT) for elemental analysis. Images were taken in bright field (BF) and dark field (DF) STEM mode (spot size: 0.7 nm), as well as in high resolution (HR) TEM mode (spot size: 1). For SEM imaging a Hitachi S-4800 was used equipped with an EDX detector. The working distance for secondary electron (SE) imaging was 8 mm, acceleration voltage 15 kV; for EDX analyses, working distance was 15 mm, acceleration voltage 20 kV.

RESULTS OF SEM IMAGING

The TEM grids with the lowest sampling time of 2 min were selected for further study, as higher sampling times resulted in quite dense samples. SEM imaging of the sampled PM from the three thrust levels examined, namely P100 (~100% power), P65 (~65% power), and P7 (~7% power) reveals the following characteristics (Figure 1 and SI Figure 2): (a) A homogeneous distribution of soot agglomerates on the TEM grids, even at relatively high magnifications of 5000, corresponding to an area of ~2 μm × 1.5 μm of the SEM image, especially for the soot-rich high thrust levels of ~100% and ~65%. (b) A diminishing trend in the amount of the soot agglomerates from the higher to the lower thrust levels. The reduction in the amount of soot agglomerates is much more pronounced between the P7 sample and the high thrust levels (P100, P65) than between the P100 and the P65 sample, for which there is no striking difference. (c) The P100 soot agglomerates are more bulky than the P65 agglomerates and the P65 ones more bulky than the P7 agglomerates. The morphological features of the soot agglomerates are further developed and discussed below, in the light of the TEM observations.

Background measurements of TEM grids exposed for 2 min (equal to the sampling time for each thrust level) reveal very rare soot agglomerates on SEM images (SI Figure 2). One soot agglomerate was found in about 30−40% of the 90 μm × 90 μm squares of the TEM grids. Higher exposure times of 5 min reveal 1−2 soot agglomerates in most squares of the TEM grids.

RESULTS OF TEM IMAGING

Low magnification TEM images of soot from the three thrust levels reveals a reduction in the size of the primary soot particle constituents of the agglomerates from the P100, through the P65 to the P7 sample (Figure 2). The size of the primary soot particles is given by the diameter of the (nearly) circular particles (projected spheres) directly measured on the TEM images with the measuring tool of the "Digital Micrograph" software.

It is generally accepted that the degree of crystallinity of the primary soot particles, which is defined according to the degree of order in the arrangement of graphene lamellae in the particle interior,[18−20] generally varies depending on the engine operating conditions, the composition of the initial fuel, the nature of gases in the exhaust stream and the ambient temperature.[20−24] Soot structure is imperfect, i.e. largely amorphous with only local development of graphene packages (referred to as crystallites), a few nm in size, with a crystalline structure. The degree of crystalline order of the primary particles is a measure of the oxidative reactivity of soot and depends on the arrangement, deformation, separation distance, and periodicity of the graphene lamellae. It should be noted that oxidation removes preferably amorphous carbon relative to graphitic carbon. Soot reactivity is also a function of the size of primary soot particles, smaller particles being more reactive than larger ones due to larger surface to volume ratio. The morphological and internal structural characteristics of soot can be modified after initial formation and oxidation.[25,26]

Soot PM at Approximate Takeoff Thrust (~100% Static Sea Level Thrust; P100). The detailed study of the individual soot particles was done after scanning parts of the grids in low magnification and localizing areas with soot

dx.doi.org/10.1021/es501809b | Environ. Sci. Technol. XXXX, XXX, XXX−XXX

agglomerates for further imaging. Soot agglomerates captured at the randomly distributed holes of the grid were preferred for imaging relative to those present on the carbon film substrate, as they show better contrast and offer the possibility of better observing the internal soot structure.

The size of the primary soot particle constituents of the agglomerates was determined on TEM images taken at magnifications of 60 000, 100 000, and 120 000, by measuring the diameter of each (nearly) circular particle (projected sphere) with the measuring tool of the "Digital Micrograph" software. Only particles with clearly distinguished outlines were chosen for the measurements. Figure 2 depicts examples about the precise way of measuring the size of the primary soot particles.

We would like to emphasize that the concept of size distribution measurements applied here (direct measurement of the diameter of primary soot particles on TEM images) is different to that followed in size distribution measurements obtained by devices such as scanning mobility particle sizers (SMPS) in aerosol science. The main differences between these two complementary approaches rely in that (a) the real time measurement devices detect and measure sizes of agglomerates and not of their primary particle constituents and (b) measurement results from such devices are characterized by rigorous statistics, as the number of measurements is very high.[16,17] In contrast, TEM imaging provides very detailed information on the particle morphology in the micro- and nanoscale on cost of rigorous statistics.

The size of the primary soot particles produced during takeoff (312 particles were measured for this thrust level) ranges between 3 and 64 nm (extreme values). About 60% of the primary soot particles are 10−25 nm in size; the most frequently measured particle sizes are between 15 and 20 nm (Figure 3), while 52% are >20 nm; the mode is 24 nm and the

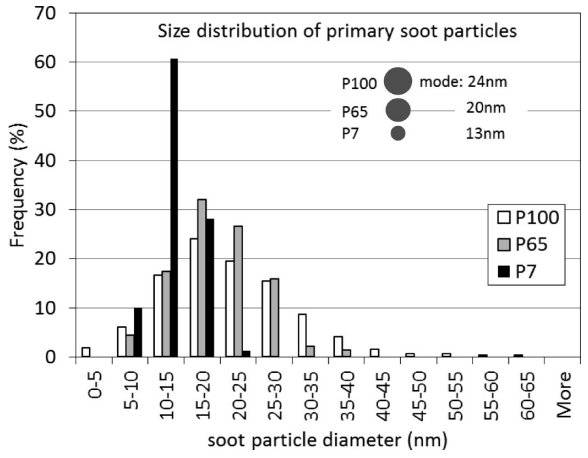

Figure 3. Histogram showing the size distribution of primary soot particles for the different engine thrust levels investigated, as measured on the TEM grids. Visualization of the mode for the three thrust levels is given in the inset.

standard deviation value is 9. The size distribution pattern is nearly normal with a slight asymmetry expressed with a positive skew (longer right tail) indicating that the percentage of larger particles (>15−20 nm) is significantly higher than that of small ones (<15−20 nm).

Primary soot particles are in their vast majority nearly spherical and strongly agglomerated (Figures 2 and 4). Single particles exposed on the sampled material in an optimum way that allows observation of their internal structure, i.e. not strongly coalesced with other particles, are rare. The particle's interior consists mostly of relatively well-ordered, curved graphene lamellae forming nearly concentric layers surrounding a number of nanometer-large cores (multicore particles) (Figure 4C, D). The cores consist of almost circular (fullerenic) or hairpin-like graphene lamellae or exhibit no lamellae in their innermost part, i.e. they are completely amorphous. The graphene lamellae surrounding the cores and making up the main part of the particle volume display deformational features such as twisting, tilting, undulations or cross-links and/or are interrupted by amorphous parts. The described structure indicates that soot particles coalesce already during early stages of formation and subsequently evolve into larger ones with longer graphene lamellae surrounding the coalesced cores. Embryonic soot particles, a few nanometers in size, are also observed attached on the outer surface of large grown particles (Figure 4D, arrow and inset). The interlamellar distance of graphene lamellae (measured only in crystallites where graphenes exhibit some periodicity) ranges mainly between 0.370 and 0.390 nm, which is significantly larger than the interlamellar distance in graphite (0.335 nm); interlamellar distances around 0.340 nm were measured in some cases in the P100 soot particles, thus indicating that development of graphitic crystalline structures is very local, an observation that is in line with previous studies.[25,27] The maximum periodicity measured in crystallites (repetition of graphene lamellae with the same interlamellar distance) is 7.

Primary soot particles with hexagonal shapes approaching the crystalline shape of graphite crystals but with round corners of the hexagons are rarely observed (Figure 4A and B). Note that the hexagonal graphene shape is observed only at the outermost particle part; no successive concentric graphene hexagons are clearly visible to build the internal structure of a considerable part of those soot particles. These features indicate that some soot particles develop nearly graphitic crystallinity at late stages of their growth.

Soot agglomerates were analyzed by EDX for their qualitative bulk chemical composition, in order to look for chemical elements supposed to derive from metal additives in the lubricating oil.[28,29] The EDX analyses reveal that the majority of the soot agglomerates are free of metallic elements, while in a few cases some Ca, P, S, and low amounts of K were detected. These elements could originate from the lubricating oil.[30]

Soot PM at Approximate Cruising Thrust (~65% Static Sea Level Thrust; P65). The size of the primary soot particles emitted at the approximate cruising thrust (271 measurements) is on average smaller than the one emitted at takeoff conditions, ranging between 7 and 38 nm (extreme values). About 75% of the primary soot particles are 10−25 nm in size; the most frequently measured sizes are between 15 and 20 nm (Figure 3).The mode is 20 nm and the standard deviation value is 6. The size distribution pattern is similar to that observed for P100 in that it also shows an asymmetry indicating higher percentage of larger particles (>of the 15−20 nm maximum) relative to small ones (<15−20 nm). However, the percentage of particles from the P65 sample that is larger than 20 nm (46%) is lower than in the P100 particle population analyzed (52%; Figure 3).

The primary soot particles are nearly spherical and strongly agglomerated; single particles were rarely found while hexagonal ones, as those identified for the P100 samples were

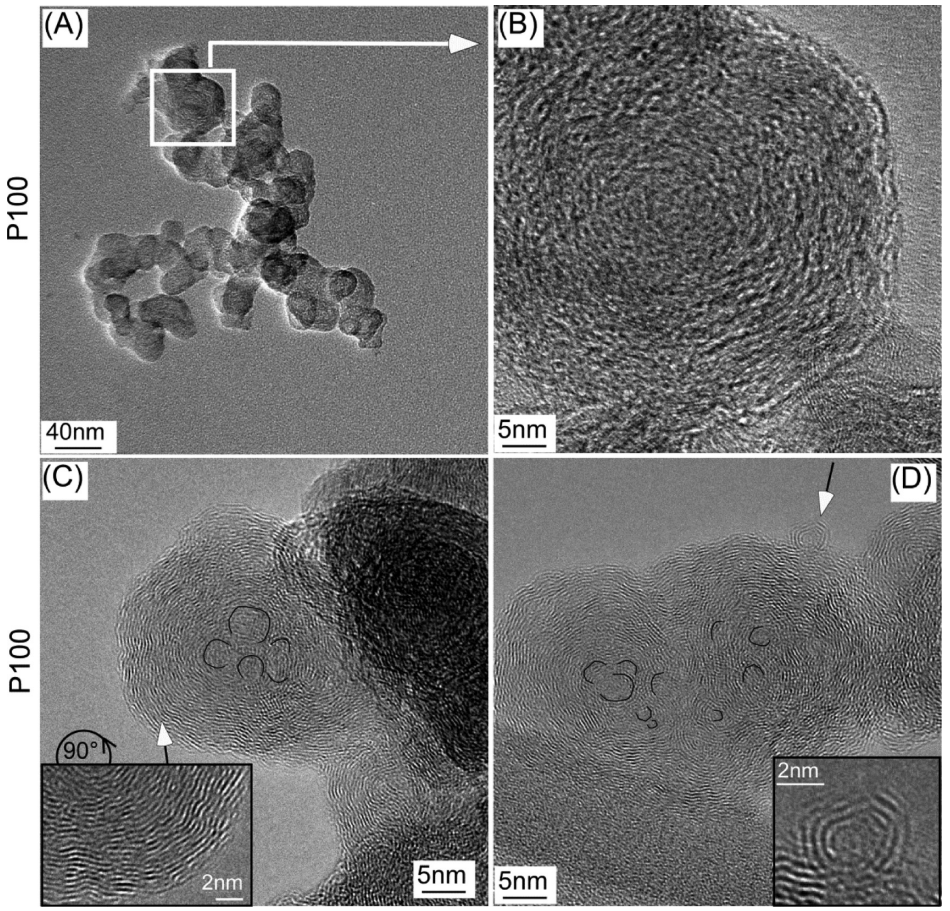

Figure 4. TEM images of soot from the P100 samples. (A) Agglomerate with nearly spherical particles and one hexagonal particle (in square) magnified in HRTEM image B. (C and D) HRTEM images of primary multicore soot particles surrounded by relatively well-ordered, deformed graphene lamellae. (C and D inset) Magnifications of parts of the images marked by arrows. The particle cores in C and D are partly outlined, for clarity.

not observed among the imaged particles. Compared to the P100 samples, the P65 soot particles seem to be a little less organized in terms of arrangement and deformational features of the graphene lamellae (degree of crystalline order) (Figure 5A, B). There are particles exhibiting locally orderly graphene lamellae arrangements (crystallites) (Figure 5B), however, less frequently than the P100 particles. Large, multicore particles with voluminous outer parts exhibit a higher degree of crystalline order than small particles. The interlamellar distance of graphene lamellae in crystallites ranges mainly between 0.390 and 0.410 nm, which is, on average, a little larger than in the P100 particles and, in any case, larger than in graphite; interlamellar distances around 0.340 nm (with a maximum periodicity of 7) were also measured indicating, like the P100 particles, the development of local graphitic crystalline structures. Based on the generally lower degree of crystalline order, as well as the generally smaller particle size, the P65 soot is characterized by a lower oxidative reactivity than the P100 soot.

Soot PM at Approximate Taxiing Thrust (~7% Static Sea Level Thrust; P7). The sizes of the primary soot particles emitted at the ~7% thrust level (321 measurements) range between 7 and 21 nm (extreme values). Here, 90% of the primary soot particles are 10−25 nm in size, and 99% of them are between 5 and 20 nm, which is significantly smaller than both P100 and P65 soot particles. The maximum percentage of particles is observed for sizes between 10 and 15 nm (Figure 3) with a mode of 13 nm and a standard deviation of 3. Also for this thrust level the size distribution pattern shows a positive skew with a higher fraction of larger particles (>of the 10−15 nm maximum) than small ones (<of the 10−15 nm maximum) but the percentage of particles that are larger than the 10−15 nm maximum is the lowest among all thrust levels analyzed (Figure 3). No particles larger than 25 nm were measured in this sample. The significantly lower size of the primary soot particles of the P7 agglomerates relative to that of higher thrust levels concurs with the SEM and TEM observation (Figures 1 and 2) that the P7 soot agglomerates are significantly less bulky than those produced under ~65% and ~100% thrust. The presence of less bulky agglomerates with smaller primary particle constituents implies a higher surface to volume ratio, which in turn points to a higher capacity for oxidation of the P7 relative to P65 and P100 soot, as far as the size of the primary particles is concerned.

Primary soot particles of the P7 samples are nearly spherical, strongly agglomerated, and even more disorganized in terms of graphene lamellae arrangement and deformational features than those of the P100 and P65 samples (Figure 5C and D). Very small particles not agglomerated and not evolved to large ones exhibit partly almost fullerenic internal structures (Figure 5C, insets). The interlamellar distance of graphene lamellae in crystallites ranges mainly between 0.360 and 0.400 nm, but the statistics for this sample is not optimum, as the number of particles allowing measurement of interlamellar spacing is

dx.doi.org/10.1021/es501809b | Environ. Sci. Technol. XXXX, XXX, XXX−XXX

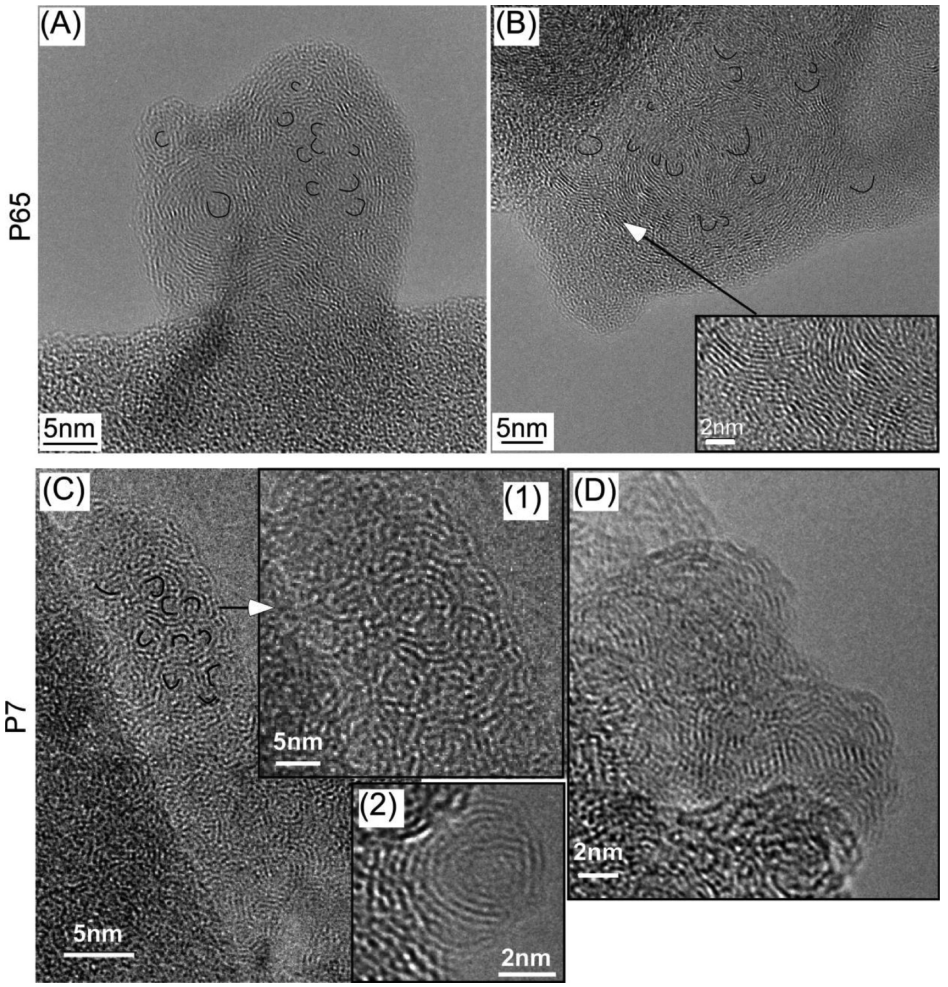

Figure 5. HRTEM images of soot from the P65 (A and B) and P7 (C and D) samples illustrating primary multicore soot particles. In the P65 samples, soot particles are larger, in contrast to the P7 soot where cores did not evolve to large particles. The particle cores are partly outlined, for clarity. (C inset 1) Magnification of part of the image. (inset 2) Single embryonic primary soot particle.

relatively low. It is worth mentioning, however, that interlamellar distances around 0.340 nm, i.e. close to the graphitic value were measured indicating the development of local graphitic crystalline structures also for the P7 soot particles. The maximum periodicity measured in crystallites is 5. The lower degree of crystalline order, in combination with the smaller particle size of P7 soot, indicates that soot produced during taxiing is more reactive than in the P100 and P65 samples.

COMPARISON OF ELECTRON MICROSCOPIC RESULTS AND ONLINE NONVOLATILE PM MEASUREMENTS

The reduction of the primary soot particle size with diminishing thrust level indicated by electron microscopy concurs with the real-time measurements of both the particle number and particle mass concentration (Table 1, Figure 6A and B).

Based on the results of the primary particle size distribution (Figure 3) we calculated the minimum soot volume produced (per cubic centimeter) for each thrust level in the 2 min sampling time. To this end, we used the mode of the particle diameter for each thrust (primary particle diameter for P7:13 nm, for P65:20 nm, and for P100:24 nm) multiplied by the corresponding particle number concentration of the real time measurements (Figure 6C, Table 1). The calculated volume refers to just one primary particle and should therefore be considered as a minimum value. Comparison of Figure 6A−C shows that the TEM-based results on the particle volume calculation show an analogous trend for the different thrust levels as the real time measurements, in that the particle volume derived for P100 is considerably higher than that for P65 and P7. A parameter that is uncertain and should be considered in the above comparison is possible variations in the amount of primary particles composing the agglomerates of each thrust level. Moreover, differences in the density of the primary soot particles produced by the different thrusts are also possible. It is expected that the P100 soot particles have a higher density compared to P65 and P7 because they show a higher degree of crystallinity (see above, section Results of TEM Imaging).

DISCUSSION

The results of this work reveal that (a) the amount of soot, (b) the size of the primary soot particles, and (c) the oxidative reactivity of soot produced during aircraft engine combustion correlate well with the thrust level of the engine tested. The soot volume produced under ∼100% engine thrust conditions, as calculated on the basis of TEM imaging, is significantly higher than under ∼65%, while at ∼7% conditions the generated soot volume is extremely low compared to ∼65%

dx.doi.org/10.1021/es501809b | Environ. Sci. Technol. XXXX, XXX, XXX−XXX

Table 1. Real Time Measurements of Particle Number, Mass Concentration, and Soot Volume Calculated from Primary Soot Particle Sizes, Based on TEM Imaging and the Measured Particle Number Concentration[a]

static engine thrust level	P7	P65	P100
measured diluted number concentration [cm^{-3}]	7.35×10^{4}	1.36×10^{6}	1.78×10^{6}
measured diluted mass concentration [mg m^{-3}]	9.00×10^{-4}	6.41×10^{-2}	2.08×10^{-1}
dilution factor	10.06	9.12	8.76
calculated exhaust number concentration [m^{-3}]	7.39×10^{11}	1.24×10^{13}	1.56×10^{13}
calculated exhaust mass concentration [g m^{-3}]	9.05×10^{-6}	5.84×10^{-4}	1.82×10^{-3}
number emission index [kg^{-1}]	5.74×10^{13}	5.67×10^{14}	5.84×10^{14}
mass emission index [g kg^{-1}]	7.04×10^{-4}	2.67×10^{-2}	6.83×10^{-2}
volume of primary soot particles [nm^3] for mode 13, 20, and 24 nm	1150	4189	7238
calculated minimum volume of primary soot particles produced in 2 min [nm^3 cm^{-3}]	8.45×10^{7}	5.70×10^{9}	1.29×10^{10}

[a]The correction factor due to line losses is expected to range between 1.5 and 1.8, for mass, and 2.5 and 7, for number.

and especially to ∼100% thrust. This inference is in line with the real-time measurements.

The amount of soot produced during combustion is generally governed by two important parameters, which vary with thrust level: (a) the frequency of occurrence of fuel-rich domains, which strongly depends on the average air to fuel ratio (AFR) and (b) the residence time of fuel in the high temperature zones of the combustion chamber, which should be kept small so that the soot produced is least. However, the factor residence time should be considered with caution, as at high thrust levels, for instance, although the residence time is small, the amount of produced soot is high, due to the very high quantities of injected fuel. Soot is also mitigated by more evenly mixing the fuel with air. AFR values clearly drop with increasing thrust level.

In addition, an efficient soot oxidation can be achieved when the fuel-stream velocity is smaller than the airstream velocity.[31] This condition does not apply for high thrust levels, resulting in lower soot oxidation and thus higher soot emissions during e.g. aircraft takeoff. Also the residence time of the produced soot in the combustion chamber is lower at higher thrust levels (due to high flow rates) than at low thrust levels (where flow rates are low). As a result, the produced soot spends less time in oxygen-rich and high-temperature surroundings under high thrust conditions, which lowers the amount of oxidized soot.

The difference in size of the primary soot particles identified here among the different thrust levels is interpreted as follows: at low thrust levels, the AFR and residence time of fuel are high, i.e. there are more oxygen-rich domains and more time available for oxidizing the produced soot. Therefore, at low thrusts both of these factors (AFR and fuel residence time) prevent the primary soot particles from growing larger by continuously burning off soot, which otherwise would deposit on the outer surface of existing embryonic particles, as is the case for soot particles observed under cruising (∼65%) and takeoff (∼100%) conditions.

As for the oxidative reactivity of soot, the present study shows that the most reactive soot (smallest and least ordered primary particles) is produced during taxiing (∼7% thrust) and the least reactive one (best ordered graphene lamellae and largest particles) during takeoff conditions (∼100% thrust). It is important to note that oxidation preferably removes (a) smaller (higher surface to volume ratio) than larger particles and (b) amorphous carbon relative to (nearly) graphitic carbon. An increase in the degree of graphene lamellae ordering of soot particles with engine thrust level has also been described for a CFM56-3 aircraft engine.[15] The increase in the degree of crystallinity (with respect to ordering of graphene lamellae and percentage of crystallites in the primary soot particles) with engine thrust is probably a result of higher temperatures prevailing at high thrust levels. Temperature is a principal parameter controlling the degree of ordering of graphene lamellae,[22] as it can cause desorption of volatiles and reorientation of the carbon chains to less disorganized structures with an increased basal plane site occupation by carbon atoms and thus decreased oxidative reactivity.[24]

The presence of very small primary soot particles in the aircraft engine exhaust at all thrust levels (especially at taxiing conditions) raise environmental and health concerns and merit further research. It is notable that the differences in morphological characteristics (size and internal structure of primary particles, as well as bulkiness of agglomerates) are much stronger between the P7 soot and the higher thrust levels (P65 and P100) than between P65 and the P100 soot. This

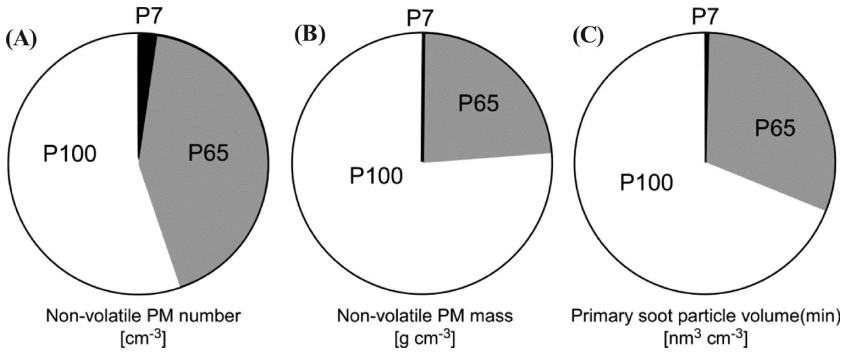

Figure 6. Graphical representation of the online measurements of nonvolatile PM number (A) and mass (B) versus static engine thrust level (time of measurements: 2 min) showing a clear correlation with thrust level. (C) Illustration of the minimum volume of soot produced during the different thrust levels, calculated on the basis of TEM-measured primary particle sizes and the online measured particle number, depicting a trend comparable to the one obtained by online measurements shown in parts A and B.

dx.doi.org/10.1021/es501809b | Environ. Sci. Technol. XXXX, XXX, XXX−XXX

observation implies that the soot produced in airport areas during taxiing shows a significantly stronger capacity to oxidation (smallest and most amorphous primary particles and least bulky agglomerates) relative to the P65 and P100 soot.

■ ASSOCIATED CONTENT

Supporting Information

Detailed description of the sampling procedure, one table with the engine settings analyzed in this study (SI Table 1), one figure depicting the sampling setup (SI Figure 1), and one figure with SEM images comparing overviews for the three engine thrust levels and background measurements (SI Figure 2). This material is available free of charge via the Internet at http://pubs.acs.org/.

■ AUTHOR INFORMATION

Corresponding Author

*Tel.: +41 58 7654190. Fax: +41 58 7654041. E-mail: anthi.liati@empa.ch.

Notes

The authors declare no competing financial interest.

■ ACKNOWLEDGMENTS

This research would not have been possible without the expertise and financial support of the Swiss Federal Office of Civil Aviation (FOCA) project "Particulate Matter and Gas Phase Emission Measurement of Aircraft Engine Exhaust". Contributors to the APRIDE 5 campaign also include the European Aviation Safety Agency, the US Federal Aviation Administration, and Transport Canada. Special thanks go to Theo Rindlisbacher, FOCA, for his technical and scientific input and to Frithjof Siegerist and his team at SR Technics Company for engine operation and test cell facility access. B.T.B. further acknowledges the financial support of Swiss Federal Laboratories for Materials Science and Technology Empa postdoc fellowship.

■ REFERENCES

(1) Lee, D. S.; Pitari, G.; Grewe, V.; Gierens, K.; Penner, J. E.; Petzold, A.; Prather, M. J.; Schumann, U.; Bais, A.; Berntsen, T.; Iachetti, D.; Lim, L. L.; Sausen, R. Transport impacts on atmosphere and climate: Aviation. *Atmos. Environ.* **2010**, *44* (37), 4678−4734.

(2) Webb, S.; Whitefield, P. D.; Miake-Lye, R. C.; Timko, M. T.; Thrasher, T. G. *Research needs associated with particulate emissions at airports*; National Academies Press: Washington, D.C., 2008, ACRP Report 6.

(3) Hansen, J.; Sato, M.; Ruedy, R.; Lacis, A.; Oinas, V. Global warming in the twenty-first century: An alternative scenario. *Proc. Natl. Acad. Sci. U.S.A.* **2000**, *97* (18), 9875−9880.

(4) Jacobson, M. Z. Control of fossil-fuel particulate black carbon and organic matter, possibly the most effective method of slowing global warming. *Journal of Geophysical Research: Atmospheres* **2002**, *107* (D19), 4410.

(5) Bond, T. C.; Sun, H. Can Reducing Black Carbon Emissions Counteract Global Warming? *Environ. Sci. Technol.* **2005**, *39* (16), 5921−5926.

(6) Sgro, L. A.; Simonelli, A.; Pascarella, L.; Minutolo, P.; Guarnieri, D.; Sannolo, N.; Netti, P.; D'Anna, A. Toxicological Properties of Nanoparticles of Organic Compounds (NOC) from Flames and Vehicle Exhausts. *Environ. Sci. Technol.* **2009**, *43* (7), 2608−2613.

(7) ICAO. Annex 16 to the Convention on International Civil Aviation: Environmental Protection. In *Vol. II−Aircraft Engine Emissions*, third ed.; ICAO: Montréal, Quebec, Canada, 2008.

(8) E-31 Aircraft Exhaust Emissions Measurement Committee. *Procedure for the Continuous Sampling and Measurement of Non-Volatile Particle Emissions from Aircraft Turbine Engines*; SAE International, 2013; AIR 6241, 2013-11-18.

(9) Anderson, B. E.; Cofer, W. R.; Bagwell, D. R.; Barrick, J. W.; Hudgins, C. H.; Brunke, K. E. Airborne observations of aircraft aerosol emissions I: Total nonvolatile particle emission indices. *Geophys. Res. Lett.* **1998**, *25* (10), 1689−1692.

(10) Herndon, S. C.; Onasch, T. B.; Frank, B. P.; Marr, L. C.; Jayne, J. T.; Canagaratna, M. R.; Grygas, J.; Lanni, T.; Anderson, B. E.; Worsnop, D.; Miake-Lye, R. C. Particulate emissions from in-use commercial aircraft. *Aerosol Sci. Technol.* **2005**, *39* (8), 799−809.

(11) Kinsey, J. S.; Dong, Y. J.; Williams, D. C.; Logan, R. Physical characterization of the fine particle emissions from commercial aircraft engines during the Aircraft Particle Emissions eXperiment (APEX) 1−3. *Atmos. Environ.* **2010**, *44* (17), 2147−2156.

(12) Lobo, P.; Hagen, D. E.; Whitefield, P. D.; Alofs, D. J. Physical characterization of aerosol emissions from a commercial gas turbine engine. *Journal of Propulsion and Power* **2007**, *23* (5), 919−929.

(13) Petzold, A.; Fiebig, M.; Fritzsche, L.; Stein, C.; Schumann, U.; Wilson, C. W.; Hurley, C. D.; Arnold, F.; Katragkou, E.; Baltensperger, U.; Gysel, M.; Nyeki, S.; Hitzenberger, R.; Giebl, H.; Hughes, K. J.; Kurtenbach, R.; Wiesen, P.; Madden, P.; Puxbaum, H.; Vrchoticky, S.; Wahl, C. Particle emissions from aircraft engines - a survey of the European project PartEmis. *Meteorologische Zeitschrift* **2005**, *14* (4), 465−476.

(14) Kinsey, J. S.; Hays, M. D.; Dong, Y.; Williams, D. C.; Logan, R. Chemical Characterization of the Fine Particle Emissions from Commercial Aircraft Engines during the Aircraft Particle Emissions eXperiment (APEX) 1 to 3. *Environ. Sci. Technol.* **2011**, *45* (8), 3415−3421.

(15) Vander Wal, R. L.; Bryg, V. M.; Huang, C.-H. Aircraft engine particulate matter: Macro- micro- and nanostructure by HRTEM and chemistry by XPS. *Combust. Flame* **2014**, *161* (2), 602−611.

(16) Schreiber, D.; Forss, A. M.; et al. *Particle Characterisation of Modern CNG, Gasoline and Diesel Passenger Cars*; SAE International, 2007; 2007-24-0123.

(17) Zervas, E.; Dorlhène, P. Comparison of Exhaust Particle Number Measured by EEPS, CPC, and ELPI. *Aerosol Sci. Technol.* **2006**, *40* (11), 977−984.

(18) Boehman, A. L.; Song, J.; Alam, M. Impact of Biodiesel Blending on Diesel Soot and the Regeneration of Particulate Filters. *Energy Fuels* **2005**, *19* (5), 1857−1864.

(19) Hays, M. D.; Vander Wal, R. L. Heterogeneous Soot Nanostructure in Atmospheric and Combustion Source Aerosols. *Energy Fuels* **2007**, *21* (2), 801−811.

(20) Song, J.; Alam, M.; Boehman, A. L.; Kim, U. Examination of the oxidation behavior of biodiesel soot. *Combust. Flame* **2006**, *146* (4), 589−604.

(21) Lapuerta, M.; Martos, F. J.; Herreros, J. M. Effect of engine operating conditions on the size of primary particles composing diesel soot agglomerates. *J. Aerosol Sci.* **2007**, *38* (4), 455−466.

(22) Su, D. S.; Müller, J. O.; Jentoft, R. E.; Rothe, D.; Jacob, E.; Schlögl, R. Fullerene-like soot from EuroIV diesel engine: consequences for catalytic automotive pollution control. *Top. Catal.* **2004**, *30−31* (1−4), 241−245.

(23) Vander Wal, R. L.; Bryg, V. M.; Hays, M. D. Fingerprinting soot (towards source identification): Physical structure and chemical composition. *J. Aerosol Sci.* **2010**, *41* (1), 108−117.

(24) Vander Wal, R. L.; Yezerets, A.; Currier, N. W.; Kim, D. H.; Wang, C. M. HRTEM Study of diesel soot collected from diesel particulate filters. *Carbon* **2007**, *45* (1), 70−77.

(25) Liati, A.; Dimopoulos Eggenschwiler, P.; Schreiber, D.; Zelenay, V.; Ammann, M. Variations in diesel soot reactivity along the exhaust after-treatment system, based on the morphology and nanostructure of primary soot particles. *Combust. Flame* **2013**, *160* (3), 671−681.

(26) Song, J.; Alam, M.; Boehman, A. L. Impact of alternative fuels on soot properties and DPF regeneration. *Combust. Sci. Technol.* **2007**, *179* (9), 1991−2037.

(27) Yehliu, K.; Vander Wal, R. L.; Boehman, A. L. Development of an HRTEM image analysis method to quantify carbon nanostructure. *Combust. Flame* **2011**, *158* (9), 1837−1851.
(28) Bardasz, E. A.; Cowling, S.; Panesar, A.; Durham, J.; Tadrous, T. N. *Effects of Lubricant Derived Chemistries on Performance of the Catalyzed Diesel Particulate Filters*. SAE International, 2005; 2005-01-2168.
(29) Sappok, A. G.; Wong, V. W. *Detailed chemical and physical characterization of ash species in diesel exhaust entering aftertreatment systems*; SAE International, 2007; 2007-01-0318.
(30) van Netten, C. Multi-elemental analysis of jet engine lubricating oils and hydraulic fluids and their implication in aircraft air quality incidents. *Science of The Total Environment* **1999**, *229* (1−2), 125−129.
(31) Lin, K. C.; Faeth, G. M. Hydrodynamic suppression of soot emissions in laminar diffusion flames. *Journal of Propulsion and Power* **1996**, *12* (1), 10−17.